Available online at www.sciencedirect.com

ScienceDirect

journal homepage: www.elsevier.com/locate/he

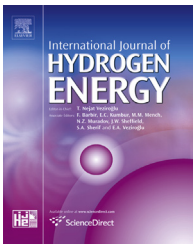

Mechanisms of NO formation in MILD combustion of CH_4/H_2 fuel blends

P. Li [a], F. Wang [a], J. Mi [a,b,*], B.B. Dally [c], Z. Mei [a], J. Zhang [a], A. Parente [d]

[a] State Key Laboratory of Turbulence and Complex Systems, Department of Energy & Resources Engineering, College of Engineering, Peking University, Beijing, 100871, China
[b] College of Energy & Power Engineering, Changsha University of Science and Technology, Changsha, 410004, China
[c] Centre of Energy Technology & School of Mechanical Engineering, The University of Adelaide, SA, 5005, Australia
[d] Service d'Aéro-Thermo-Mécanique, Université Libre de Bruxelles, Bruxelles, 1050, Belgium

ARTICLE INFO

Article history:
Received 12 June 2014
Received in revised form
2 September 2014
Accepted 9 September 2014
Available online 7 October 2014

Keywords:
MILD combustion
Flameless oxidation
Hydrogen
NO_x

ABSTRACT

The mechanisms of formation and destruction of NO in MILD combustion of CH_4/H_2 fuels blends are investigated both experimentally and numerically. Experiments are carried out at a lab-scale furnace with the mass fraction of hydrogen in fuel ranging from 0% to 15%; furnace temperature, extracted heat and exhaust NO_x emissions are measured. Detailed chemical kinetics calculations utilizing computational fluid dynamics (CFD) and well-stirred reactor (WSR) are performed to better analyze and isolate the different mechanisms.

When the MILD combustion of the CH_4/H_2 fuel is established in experiments, the thermal field is quasi uniform and the high temperature zone is located at the junction of the fuel and air jets. As the mass fraction of hydrogen in fuel is increased from 5.7% to 14.4%, although the furnace average temperature is increased, the NO_x emission remains unchanged. This cannot be explained by the thermal NO mechanism. CFD and WSR simulations both suggest that, when equivalence ratio $\leq$0.8, the N_2O-intermediate route controls the NO formation and the NO-reburning reaction is also strong. With the hydrogen addition, the importance of the NNH route is increased but that of the prompt route is decreased, consequently non-affecting the NO_x emission as measured.

Chemical kinetics calculations indicate that the conversion from NO to NO_2 becomes significant and thus the relative importance of NO_2 is increased in the total NO_x emission under low temperature MILD conditions. As the reactor temperature is increased from 1100 K to 1600 K, the importance of N_2O route decreases while that of thermal route increases. In contrast, as the initial mass fraction of oxygen is increased from 3% to 9%, the importance of N_2O route increases but that of the prompt and NNH routes decreases. Likewise, as the equivalence ratio increases, the NO-reburning reaction becomes strong. Worth noting is that the N_2O-intermediate route controls the NO production under fuel lean conditions whereas the prompt route is dominant in rich ones.

* *Corresponding author*. State Key Laboratory of Turbulence and Complex Systems, Department of Energy & Resources Engineering, College of Engineering, Peking University, Beijing, 100871, China. Tel./fax: +86 01062767074.
E-mail address: jcmi@coe.pku.edu.cn (J. Mi).

http://dx.doi.org/10.1016/j.ijhydene.2014.09.050

Nomenclature

Symbols

A_i	pre-exponential factor
C_ξ	the volume fraction constant of eddy dissipation concept model (=2.1377)
C_τ	the time scale constant of eddy dissipation concept model
D_a	diameter of the air nozzle exit, mm
D_f	diameter of the fuel nozzle exit, mm
K_v	gas recirculation rate
p	pressure, atm
$Q_{extracted}$	extracted heat, kW
Q_{input}	thermal input, kW
T	temperature, K
$T_{average}$	average temperature of the furnace centerline, K
$T_{exhaust}$	exhaust temperature, K
T_{mean}	mean temperature of the entire furnace, K
T_{WSR}	temperature of the well-stirred reactor, K
X_{NO_x}	NO_x emission in volume, ppm
Y_{CH_4}	initial mass fraction of CH_4 in the well-stirred reactor, %
Y_{CO_2}	mass fraction of CO_2, %
$Y^f_{H_2}$	initial mass fraction of H_2 in fuel, %
Y_{H_2}	initial mass fraction of H_2 in the well-stirred reactor, %
Y_j	the mass fraction for the jth species, %
Y_{N_2}	initial mass fraction of N_2 in the well-stirred reactor, %
Y_{O_2}	initial mass fraction of O_2 in the well-stirred reactor, %
$Y^o_{O_2}$	initial mass fraction of O_2 in oxidant, %

Greek letters

ξ	characteristic length fraction of fine scales, m
τ	residence time, s
Φ	equivalence ratio

Introduction

Binary fuel blends are widely used in developing high efficiency and low emission combustion devices [1]. Adding hydrogen to methane (or natural gas) can promote ignition and enhance flame stability [2–5], and offer definite advantages in applications such as combustion furnaces and engines [6,7]. However, the hydrogen addition generally increases the flame temperature and thus yields more NO_x emissions. To solve this problem, one of the effective methods is to operate the combustion in moderate or intense low oxygen dilution (MILD) condition to suppress NO_x emissions [8–10].

The MILD combustion is achieved by strong exhaust gases recirculation, where reactants are intensely diluted and hence reactions occur volumetrically without visible flame-front. Relative to the conventional counterpart, the MILD combustion increases the in-furnace thermal uniformity and efficiency, and simultaneously suppresses NO_x emission [11–14]. Although considerable work has been published on MILD combustion [14–28], most of the previous investigations have focused on firing hydrocarbon gaseous fuels or pulverized coal. To understand the characteristics of the MILD combustion of hydrogen containing fuels, both the experimental and numerical investigations are essential.

In Table 1 a summary of published experimental work on the MILD combustion of the CH_4/H_2 fuel in furnaces is presented. Derudi et al. [29,30] showed that, relative to burning pure CH_4, the MILD combustion of the CH_4/H_2 fuel requires higher jet velocity to establish, but it can operate at lower average furnace temperatures. They also found that the addition of hydrogen leads to complete oxidation of the hydrocarbon under MILD conditions. Parente et al. [31] carried out numerical and experimental investigations of the MILD combustion of the CH_4/H_2 fuel (with hydrogen content up to 20% by wt.). For their MILD combustion system, they discovered that the influence of molecular diffusion should be considered in the numerical prediction of H_2 distribution, but its effects on the temperature field and major species are negligible. They also developed a simple NO formation mechanism based on the thermal and prompt routes to predict NO emissions. The MILD combustion in their experiments notably operated in relatively high temperatures (>1800 K). Parente et al. [32] further developed a simplified approach to predict NO formation in the MILD combustion of CH_4/H_2 mixtures. They found that the NNH and N_2O-intermediate routes are crucial when the MILD combustion occurs at low temperatures and hydrogen is added to the fuel. Arghode et al. [33] found that the addition of H_2 results in a slight increase of the NO emission for the same equivalence ratio possibly due to a higher flame temperature. Galletti et al. [34] pointed out

Table 1 – Summary of experimental investigations on the MILD combustion of the CH_4/H_2 fuel in furnaces.

Fuel	$Y^f_{H_2,W_2}$ (%)	T_a (K)	P (kW)	NO_x emissions (ppm)	CO emissions (ppm)	Reference
CH_4/H_2 mixture	5, 15	≥1173	0.2–0.3	<30	<50	[29]
CH_4/H_2 mixture	15	≥1173	0.2–0.3	<30	<50	[30]
CH_4/H_2 mixture	5.5	800–900	13	59–105	N/A	[31]
CH_4/H_2 mixture	50	N/A	10	25–45	N/A	[32]
CH_4/H_2 mixture	8	300	6.25	0–30	20–600	[33]
CH_4/H_2 mixture	15	1223, 1312	0.2–0.3	17	<50	[34]
CH_4/H_2 mixture	0–100	298, 858	20	8–16, 26–42	3–60, ≤10	[35]

that, for the MILD combustion operating in 1300–1400 K, the NNH and N_2O-intermediate routes are the dominant formation pathways for the MILD combustion of CH_4/H_2 mixtures. Ayoub et al. [35] carried out MILD combustion experiments in a laboratory-scale furnace (20 kW) and found that MILD combustion can be established for CH_4/H_2 mixtures whatever the mass fraction of H_2 and even when pure H_2 was used. In their experiment, with the addition of H_2, the NO_x emission was decreased due to the decrease of prompt NO route. Yu et al. [36] performed a well-stirred reactor (WSR) network simulation on the MILD combustion of CH_4/H_2 mixtures. They found that CO decreases from 48 ppm to zero when the volume fraction of H_2 is increased from 40% to 100%, but the NO_x emission is not changed significantly. They also discovered that the NO_x and CO emissions do not depend on the exhaust gas recirculation in the highly diluted conditions.

In addition to studies in furnaces, the investigation of MILD combustion was also performed using jet-in-hot-coflow burner which emulates the MILD combustion regime locally in furnace [23,37,38]. Medwell et al. [39] carried out laser diagnostic experiments using a jet-in-hot-coflow burner operating at MILD conditions. Their experiments demonstrated that H_2 addition to the primary fuel can stabilize the flame, but the structure of the reaction zone is not varied significantly. Mardani et al. [40] numerically investigated the CH_4/H_2 jet in hot and diluted coflow air flame under the MILD condition. These authors revealed that the hydrogen addition to methane increases reaction rates. Mardani et al. [41] also pointed out that the NNH and N_2O-intermediate routes are most important pathways in NO formation under MILD conditions. Moreover, they discovered that, as the hydrogen level is decreased, the importance of the NNH and N_2O-intermediate routes decreases. The investigation of Gao et al. [42] indicated that the NNH and prompt routes play a significant role in the NO formation under the MILD conditions of CH_4/H_2 mixtures using the jet-in-hot-coflow burner. It is worth noting that the mass fraction of the oxygen in the hot coflow is not low (9%). Their results also revealed that the NO formation is suppressed as the mass fraction of hydrogen is decreased. Sepman et al. [43] investigated the effect of hydrogen addition on the flame structure of MILD condition using a laminar-jet-in-hot-coflow burner. They found that the addition of hydrogen substantially decreases the flame height (~25%) but only slightly affects the maximal flame temperature and the thickness of combustion zone. Afarin et al. [44] examined the effect of hydrogen addition on the CH_4/H_2 flame structure under the MILD condition using large eddy simulation. These investigators concluded that the addition of hydrogen to fuel not only increases both the peak temperature and the flame thickness but also reduces the fluctuation of the OH radical and the diffusion of the un-burnt fuel in the flame front.

The previous studies cited above have preliminarily investigated the NO formation mechanisms under the MILD combustion of CH_4/H_2 fuel blends. However, no systematical work has been conducted that examines the effects of various operational parameters (i.e., the hydrogen addition, temperature, oxygen level, and equivalence ratio) on the formation routes of NO. The present study is our effort to help address this issue. Two specific objectives are designated: (1) to experimentally investigate the effect of hydrogen addition on the performance of MILD combustion, and (2) to numerically examine the NO mechanism of the MILD combustion of CH_4/H_2 mixtures systematically. For the first objective, experiments are performed at the mass fraction of hydrogen in fuel ranging from 0% to 15%. The flow field, furnace temperature, extracted heat and exhaust NO_x emissions are obtained. For the second objective, the NO mechanism is investigated by CFD and WSR simulations. In particular, effects of hydrogen addition, reactor temperature, oxygen level, and equivalence ratio on the NO formation and reduction mechanisms under the MILD condition of CH_4/H_2 mixtures are investigated. Finally, the effect of kinetic scheme on NO mechanism is analyzed.

Research methods

Experimental setup

The experiments are carried out at a laboratory-scale Adelaide MILD combustion furnace and details of which have been given in ref. [45,46]. The combustion chamber is well insulated and allows only ~20% of the total heat input to be conducted through the walls. As a result, it usually takes a warm-up time of about 1.5 h from a cold state to steady-state operation. There are five openings accommodating interchangeable insulating window plugs or UV grade fused silica windows. The five openings are equally spaced vertically down three sides of the furnace. To control the heat load, two U-shaped cooling tubes with variable heat exchange areas are used. The heat exchangers can be inserted through any of the window openings. For this investigation their exposed surface areas are 0.03 m^2 each. These heat exchangers remove 4.46 kW and 4.93 kW of heat on average for the firing rates of 10 kW and 15 kW, respectively.

The time-averaged furnace temperature is measured with a bare, fine-wire, type R (Pt–Pt–13%Rh) thermocouple of 254 μm diameter wire with a bead diameter of 1.2 mm under steady-state conditions. Five measurement points along the axial centerline of the furnace are selected as temperature measurement locations. The exhaust temperature is measured with a stainless steel sheath type K (Ni–Cr) thermocouple. Exhaust emissions of NO, NO_2, CO_2 and O_2 are measured using a TESTO 350 XL portable gas analyzer. While uncertainties of the mean temperatures measured by thermal couples are about ±4 K, the analyzer measurement accuracies are estimated to be: [NO] = ±5 ppm and [NO_2] = ±5 ppm. The analyzer is checked with a calibration gas to yield total NO_x emissions accuracies better than ±5 ppm. Total NO_x emission ($NO + NO_2$) concentrations are reported by volume on a dry basis corrected to 3% O_2 concentration. By correcting to a specific O_2 level, true comparisons of emissions levels can be made because the effect of various degrees of dilutions has been removed, while still retaining a familiar mole-fraction-like variable.

The burner consists of a single fuel nozzle on the axis of the furnace, and four exhaust and four air ports arrange symmetrically in a ring pattern on the same wall. The schematic figure of the MILD combustion furnace can be found in ref. [45]. The inner diameter of the central fuel nozzle and four air

nozzles is $D_f = 7.2$ and $D_a = 4.0$ mm, respectively. In the present experiments, the room-temperature reactants (≈288 K) are injected into the furnace and the equivalence ratio (Φ) of 0.8 is used and kept constant. The furnace is operated with a thermal input of 13 kW when only natural gas (NG) is used as fuel. The NG supply is kept constant. With the addition of hydrogen, the mass fraction of hydrogen in the fuel jet (NG/H_2) is increased from 0% to 14.4% (by mass) and the thermal input is increased from 13 kW to 19.1 kW. The properties and composition of natural gas used in the present experiment is shown in Table 2.

To our best knowledge, there are four kinds of definitions of the MILD combustion, i.e., (1) the definition of Wünning and Wünning [11], (2) the definition of Kumar et al. [47], (3) the definition of Cavaliere et al. [8] and (4) the definition of the present authors [45,46,48]. Wünning and Wünning [11] defined the MILD combustion regime using the global parameters of gas recirculation rate (K_v) and furnace temperature. The gas recirculation rate (K_v) is the ratio between the mass flow rate of exhaust gases internally recirculated into the air and fuel streams before reaction and the total mass flow rate injected into the furnace. The MILD combustion regime occurs when $K_v > 3$ and furnace temperature higher than 1100 K [11]. However, in general, it is extremely difficult to measure K_v by experiments, and thus the judgment of the MILD combustion is not straight-forward. Kumar et al. [47] defined the MILD combustion based on the mean square temperature fluctuation over the combustor (T'^2). T'^2 is calculated as:

$$T'^2 = \int \left(\frac{T - T_{mean}}{T_{mean}}\right)^2 dV \Big/ \int dV, \quad (1)$$

and the MILD combustion is defined as $(T'^2/T_{mean}) < 15\%$. Nevertheless, it is also not easy to obtain T'^2 and T_{mean} through experiments, because the estimation of T_{mean} needs the temperature data everywhere inside the entire furnace. The MILD combustion defined by Cavaliere et al. [8] is "a combustion process when the inlet temperature of the reactant mixture is higher than mixture self-ignition temperature whereas the maximum allowable temperature increase with respect to inlet temperature during combustion is lower than mixture self-ignition temperature." This definition is based on the well-stirred reactor. The definitions of the MILD combustion of burning gaseous, liquid and solid fuels are discussed in our previous study [48]. For the present study of firing gaseous fuels, the MILD combustion in experiments is defined as the flameless combustion where no visible flame front occurs at all. Although when the MILD combustion occurs, the characteristics of the thermal and gas species fields are different from that of the conventional combustion. It is better to use a straight-forward method to judge the occurrence of MILD combustion in experiments. In the present experiments, when there is no visible flame, the measured temperature fields are semi-uniform, and the NO_x and CO emissions are lower than 40 ppm and 10 ppm, respectively. Therefore, for gaseous fuels, the MILD combustion can be indeed defined based on the appearance as the flameless combustion where no visible flame front occurs at all. The occurrence of the flameless combustion can ensure the low NO_x emission results.

CFD calculations

Computational fluid dynamic (CFD) simulations are performed to investigate the NO mechanism of MILD combustion in Cases 1–4. The modeling detail and validation can be found in Refs. [46,49–52] and only a brief description is provided below.

The commercial software FLUENT code [53] is used to model these furnace utilizing steady state, implicit, finite volume based models. The pressure velocity coupling is the SIMPLE algorithm. Full hexahedral grid (about 2000,000 hexahedral cells) is adopted to minimize the grid size and appropriate refinement of grid is performed in the regions with higher gradients. The adequacy of this mesh (i.e., the grid independence) is verified by comparing the results with those obtained using a finer grid with 4,000,000 cells. The comparison between these two cases shows a high consistency in the results. The realizable $k-\varepsilon$ model with the standard wall function is taken for modeling the turbulent flow.

The eddy dissipation concept (EDC) [54] is used with the detailed reaction mechanism of GRI-Mech 2.11 [55] to simulate the oxidation of the fuel. The EDC model is an extension of the eddy dissipation model to consider detailed chemical mechanisms in turbulent flows and can capture finite rate chemistry effects. The EDC model assumes that reactions occur at fine scales. The reaction at fine scales is assumed to occur as a constant pressure reactor. The characteristic length fraction of fine scales (ξ) and the chemical residence time scale (τ) of fluid in the fine structures is expressed by.

$$\xi = C_\xi \left(\frac{\upsilon\varepsilon}{\overline{k^2}}\right)^{1/4}, \quad \tau = C_\tau \left(\frac{\upsilon}{\varepsilon}\right)^{1/2} \quad (2)$$

where C_ξ is the volume fraction constant (=2.1377) and C_τ is the time scale constant (=0.4083). The evolutions of species concentrations are then computed by integrating the chemistry within those fine scales. In EDC model, the species conservation equation takes the following general form:

$$\frac{\partial(\rho Y_i)}{\partial t} + \nabla\cdot\left(\rho\vec{v}Y_i\right) = -\nabla\vec{J}_i + R_i \quad (3)$$

Table 2 – Properties and composition of natural gas used in the present experiment.

Fuel	LHV[b]	CH_4	C_2H_6	CO_2	N_2	C_3H_8	C_4H_{10}	C_5H_{12}	C_6H_{14}
Natural gas[a]	51.154	91.36	4.364	2.084	1.278	0.62	0.20	0.055	0.04

[a] Gas analysis provided by Origin Energy Australia.
[b] Lower heating value (MJ/kg).

where Y_i, $\vec{J}_i$ and R_i are respectively the local mass fraction of each species i, the diffusion flux and the net rate of production by chemical reaction. The chemistry source term (R_i) is computed by

$$R_i = \frac{\rho\xi^2}{\tau\left(1-\xi^3\right)}\left(Y_i^* - Y_i\right) \quad (4)$$

with Y_i^* being the fine-scale species mass fraction after reacting over the time (τ). The evolution of Y_i^* depends also on the chemical kinetic mechanism. Note that the expression (4) is only valid when the turbulence Reynolds number $Re_t > 65$ [56]. If $Re_t < 65$, the early ignition problem may occur. This problem can be avoided by modifying the EDC model constants [56,57].

Although discrepancies between the EDC simulations and experiments are notable at low oxygen levels [42,58], the similar may occur for extremely low oxygen cases if the time scale constant of the EDC model is set as $C_\tau = 0.4083$ [56,57]. Since the gradients of temperature and species are significantly lower in MILD than conventional combustion, the former should have a greater residence time in the fine structures of the EDC model than does the latter [56,57]. Moreover, the reaction rate of MILD combustion is far lower than that of conventional combustion. Therefore, C_τ should be taken greater than 0.4083 so that the simulated reaction rate is reduced. It follows that the characteristics of the MILD reaction operating at extremely low oxygen levels can be captured. Accordingly, in some of our modeling studies of the MILD combustion, especially under extremely low oxygen levels, the time scale constant is increased from $C_\tau = 0.4083$ to $C_\tau = 1.5$ or 3.0 [56,57].

For the present MILD combustion occurring in a furnace, since $Re_t > 65$ (see Ref. [46] for detail), the default values of EDC model constants of $C_\xi = 2.1377$ and $C_\tau = 0.4083$ are adopted. As shown in Section 3.2, the predicting temperature distributions agree well with experiments.

Differential diffusion is considered by representing molecular diffusion coefficients for each species as a fourth-order polynomial function of temperature. The discrete ordinate radiation model is adopted with a weight sum of gray gas model to model the radiation. Once the flow and thermal fields have been obtained from the model and validated with the experiment, the NO route paths are calculated as a post-processing operation in FLUENT [53]. The NO production typically appears in low concentrations and the NO chemistry has a negligible influence on the predicted flow field, temperatures and major combustion product concentrations and thus the post-processing operation of the NO calculation is reasonable. The thermal, prompt, N_2O-intermediate, NNH and NO-reburning mechanisms are considered in the present simulation. The O radical concentration in thermal NO and N_2O-intermediate routes, as well as the OH radical concentration in thermal NO, are predicted using the EDC model with GRI-Mech 2.11 mechanism (this method is termed as the instantaneous approach in FLUENT [53]). The prompt NO formation is modeled following De Soete [59]. The N_2O-intermediate mechanism is assumed at the quasi-steady-state [53]. The thermal, prompt and N_2O-intermediate routes are based on kinetic mechanisms with Arrhenius equations integrated over a probability density function (PDF) for temperature in order to take into account the effect of turbulent fluctuations on the mean reaction rates. For the NNH route, because there is no commercial code available, we use the EDC model with the NNH mechanism [60] to simulate its production, see ref. [45,46] for details.

Boundary conditions are velocity inlet, pressure outlet and temperature wall boundary. The temperature of wall boundary is set by using the user defined function of FLUENT [53] to be consistent with the experimental measurement. The second-order scheme is employed for pressure and the second-order upwind scheme for momentum, turbulent kinetic energy, turbulent dissipation, species transport and energy equations. Convergence is obtained when residuals are below 10^{-6} for the energy and 10^{-5} for all other variables. The outlet temperature and velocity are monitored and their variations are allowed to be within 1 K and 0.1 m/s, respectively, to achieve the convergence of their solution.

Chemical kinetics calculations

MILD combustion is characterized by intense internal recirculation and low temperature gradient inside the furnace. Theoretically, the entire in-furnace region of the MILD combustion furnace can be simplified as a large well-stirred reactor (WSR), because chemical timescales are much larger than turbulent timescales due to the relatively strong internal recirculation and dilution of the reactant [24,61]. De Joannon et al. [61] reported the similarity between concepts of MILD condition and WSR. They used the WSR to investigate the characteristics of MILD combustion regime. Mardani et al. [24] also adopted the WSR to explore the CO and CO_2 formation in CH_4/H_2 blended combustion under MILD condition. In addition, the EDC model assumes that reaction occurs in small turbulent structures (called the fine scales) and the fine scale are assumed as isobaric, adiabatic and perfectly stirred reactors [54]. Recently, Minamoto and Swaminathan [62] discovered through direct numerical simulation that the WSR-based model is appropriate for the modeling of MILD condition. Therefore, there are some qualitative similarities between characteristics of the MILD regime and the WSR. For the present study, the chemical kinetics calculation is carried out with the WSR model to investigate the NO mechanism. The WSR analysis is performed by solving the species conservations equations under constant reactor temperature over a residence time using CHEMKIN 4.1 [63].

The residence time (τ) is set as 1.00 s in the WSR model. In our preliminary calculation, the influence of τ on the reaction pathways of NO mechanism is examined. It is noticed that τ has significant influence on the elementary reaction pathways, when τ is varied from 0.01 s to 1.00 s. The reason is that the NO formation reaction is slow. By setting $\tau = 1.00$ s it is possible to ensure that the NO reaction path is near the chemical equilibrium state. It is worth noting that other researchers [64,65] also adopted the residence time in the range from 0.30 s to 1.00 s to investigate the NO formation and reburning chemistry.

It is vital to choose an appropriate chemical mechanism for the WSR calculation. GRI-Mech 2.11 is suitable for modeling the condition of roughly 1000–2500 K, 10 torr to 10 atm, and equivalence ratio from 0.1 to 5 [55]. Previous studies [66–69]

showed that the full chemical mechanism of GRI-Mech 2.11 is better than GRI-Mech 3.0 in the modeling of the NO mechanism. Therefore, GRI-Mech 2.11 is adopted in the present modeling.

The sensitivity analysis is performed to clarify the main reaction pathways for NO formation and reduction. The sensitivity analysis provides the values of the first-order sensitivity coefficients (A_i/Y_j) ($\delta Y_j/\delta A_i$). Here, A_i is the pre-exponential factor for reaction i, and Y_j is the mass fraction for the jth species. Thus, the sensitivity coefficients can be interpreted as the relative change in the predicted concentration for species j caused by increasing the rate constant for reaction i.

The MILD cases investigated

Table 3 contains a summary of all MILD condition cases. Cases 1–4 are investigated experimentally and numerically. For these cases, the furnace temperature, extracted heat and exhaust NO_x emissions are measured in the experiments, while the in-furnace flow field and NO emission are obtained by CFD. The effects of hydrogen addition (Cases 5–7), reactor temperature (Cases 8–10), oxygen level (Case 11–13) and equivalence ratio (Cases 14–16) on the NO formation and reduction mechanisms are explored by chemical kinetics calculations with the well-stirred reactor (WSR) model. For Cases 11–13, the initial oxygen mass fraction is changed and the equivalence ratio is kept constant by varying the N_2 diluting level. For Case 16, the fuel rich case is examined because there is fuel rich region existing inside the practical furnace.

Results and discussion

Experimental furnace results

In Fig. 1 the effects of adding hydrogen to the natural gas fuel stream in the MILD combustion furnace are shown. The hydrogen addition varied from 0 to 14.4% as follows; (a) $Y^f_{H_2} = 0\%$, (b) $Y^f_{H_2} = 5.7\%$ and (c) $Y^f_{H_2} = 14.4\%$. The thermal field is obtained by measuring the mean temperature using a thermocouple, while the simplified flow field is deduced from the CFD results and represented by the dashed lines on the left.

For the three cases of Fig. 1, the in-furnace temperature is semi-uniform and relatively low (≤1300 K). The temperature difference across the furnace is small, mainly less than 50 K in each case. Moreover, as the hydrogen is added to natural gas, although the furnace temperature is increased, the location of the high temperature zone does not change. From Fig. 1, it is clear that the high temperature region is located at the junction of the upward fresh fuel jet and downward recirculated air jet. The flow rate of the air jet is ten times greater than the fuel jet and thus the jet momentum of the former is significantly higher than the latter. Therefore, the strong air jet dominates the flow and entrains the weak fuel jet at the lower part of the furnace. There is a V-shaped junction region of the fuel and air jets. The MILD combustion mainly occurs in this V-shaped region and thus the temperature is relatively high in this zone (see Fig. 1). The temperature in the main reaction region increases with the addition of hydrogen. For instance, at $Y^f_{H_2} = 0\%$, the temperature at the main reaction zone is approximately 1200 K; at $Y^f_{H_2} = 5.7\%$, the temperature at the V-shaped zone is 1250 K; at $Y^f_{H_2} = 14.4\%$, it is 1300 K. Note that, although Fig. 1 only shows the two-dimensional cross section of the furnace, this section incorporates the reactants jets and so represents the most important reaction zone in the furnace.

It is also worth noting that the temperature distribution of the MILD combustion in the present experiment is different from our previous study using the same furnace, see ref. [45] for details, because the burner configuration is different. For our previous study, the burner consists of a central air jet and four side fuel jets. Therefore, the junction of the previous fuel and air jets was located around the furnace central region and thus high temperature is also over there. For the present study, a V-shaped junction region is formed by the side air jets

Table 3 – Summary of the MILD cases investigated.

Cases	Fuel	$Y^f_{H_2}$ (%)	$Y^0_{O_2}$ (%)	Φ	EXP & CFD	WSR[a]	T_{WSR}	(Y_{H_2}, Y_{CH_4}, Y_{O_2}, Y_{N_2}) in WSR
1	NG	0.0	23.0	0.8	√	–	–	–
2	NG + H_2	5.7	23.0	0.8	√	–	–	–
3	NG + H_2	10.8	23.0	0.8	√	–	–	–
4	NG + H_2	14.4	23.0	0.8	√	–	–	–
5	CH_4	0.0	3.0	0.8	–	√	1345	(0.000%, 0.597%, 2.982%, 96.421%)
6	$CH_4 + H_2$	10.0	3.0	0.8	–	√	1345	(0.054%, 0.488%, 2.984%, 96.474%)
7	$CH_4 + H_2$	20.0	3.0	0.8	–	√	1345	(0.100%, 0.398%, 2.985%, 96.517%)
8	$CH_4 + H_2$	20.0	3.0	0.8	–	√	1100	(0.054%, 0.488%, 2.984%, 96.474%)
9	$CH_4 + H_2$	20.0	3.0	0.8	–	√	1345	(0.054%, 0.488%, 2.984%, 96.474%)
10	$CH_4 + H_2$	20.0	3.0	0.8	–	√	1600	(0.054%, 0.488%, 2.984%, 96.474%)
11	$CH_4 + H_2$	20.0	3.0	0.8	–	√	1345	(0.054%, 0.488%, 2.984%, 96.474%)
12	$CH_4 + H_2$	20.0	6.0	0.8	–	√	1345	(0.108%, 0.971%, 5.935%, 92.986%)
13	$CH_4 + H_2$	20.0	9.0	0.8	–	√	1345	(0.161%, 1.229%, 8.855%, 89.535%)
14	$CH_4 + H_2$	20.0	3.0	0.5	–	√	1345	(0.034%, 0.306%, 2.990%, 96.670%)
15	$CH_4 + H_2$	20.0	3.0	1.0	–	√	1345	(0.068%, 0.609%, 2.980%, 96.343%)
16	$CH_4 + H_2$	20.0	3.0	1.5	–	√	1345	(0.101%, 0.911%, 2.970%, 96.018%)

[a] τ and p for WSR is 1 s and 1 atm, respectively.

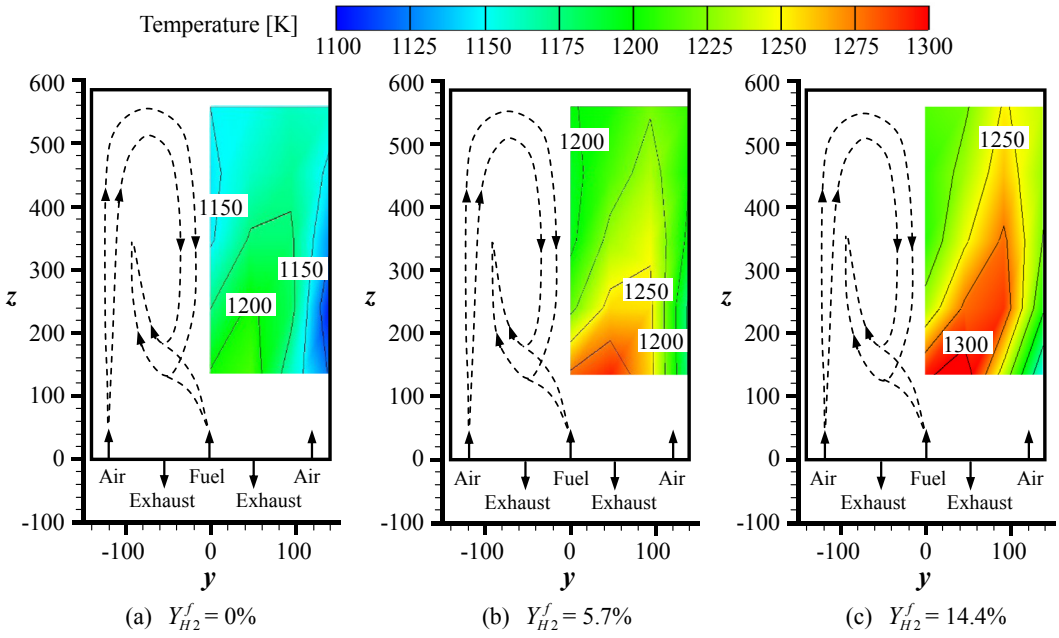

Fig. 1 – Measured furnace temperature distribution under the MILD combustion at x = 0, together with a simplified diagram of the flow field obtain from CFD. (a) $Y^f_{H_2}$ = 0%, (b) $Y^f_{H_2}$ = 5.7% and (c) $Y^f_{H_2}$ = 14.4% (Cases 1, 2, and 4).

and central fuel jet configuration. Hence the V-shaped high temperature region is formed there as shown in Fig. 1.

Fig. 2a shows the effects of hydrogen addition on the exhaust mass fraction of O_2 (Y_{O_2}) and CO_2 (Y_{CO_2}), as well as the NO_x emission (X_{NOx}, ppm in volume) while Fig. 2b displays the furnace average temperature ($T_{average}$), exhaust temperature ($T_{exhaust}$), thermal input (Q_{input}) and extracted heat ($Q_{extracted}$) versus the hydrogen addition. As the mass fraction of hydrogen in the fuel ($Y^f_{H_2}$) is increased from 0 to 14.4%, Q_{input} increases from 13.0 kW to 19.1 kW, $Q_{extracted}$ increases from 5.3 kW to 6.3 kW, and $T_{average}$ increases from 1164 K to 1232 K.

Note that $T_{average}$ is obtained by averaging temperatures along the furnace centreline. As $Y^f_{H_2}$ increases from 0 to 5.7%, the NO_x emission increases from 18 ppm to 35 ppm. However, interestingly, as $Y^f_{H_2}$ is further increased from 5.7% to 14.4%, the NO_x emission is not changed and remains constant at 35 ppm. Namely, as $Y^f_{H_2}$ is increased from 5.7 to 14.4%, both the $T_{average}$ and $Q_{extracted}$ are increased, but the NO_x emission remains unchanged. This cannot be explained by the conventional thermal NO mechanism because the previous knowledge tells that the NO_x emission is generally increased as the furnace temperature increases [10,70]. Therefore, it is

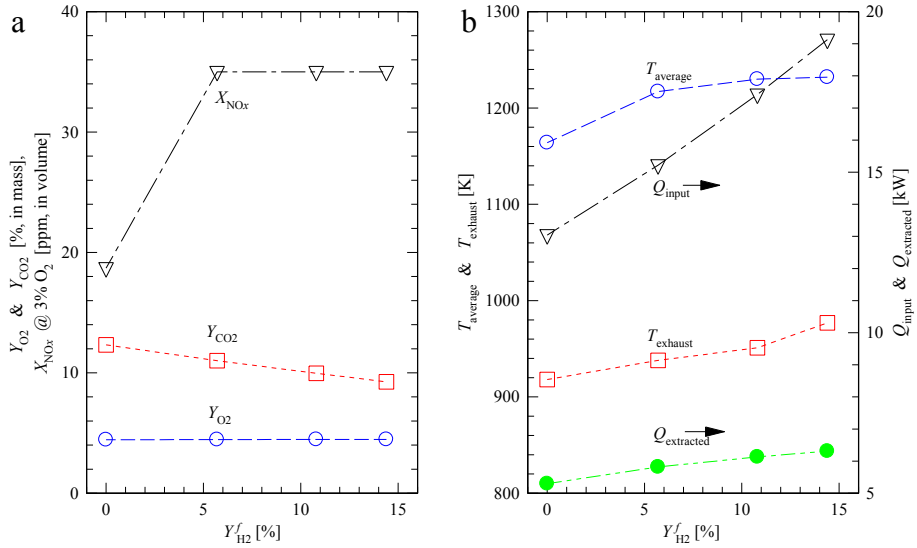

Fig. 2 – Effects of hydrogen addition on (a) the exhaust emissions of O_2, CO_2, and NO_x and (b) the furnace average temperature, exhaust temperature, thermal input, and extracted heat (Cases 1–4).

necessary to investigate the NO formation mechanism under the MILD combustion of hydrogen-containing hybrid fuels in detail, which is presented in next section. It is worth mentioning that the CO emissions for all experimental cases are too small, below the threshold of the gas analyzer, and thus not recorded. The extremely low emissions of CO for all experimental cases indicate that the fuel is completely oxidized in the experimental combustion, regardless of the hydrogen addition.

CFD results

In this Section, CFD results are presented in order to investigate the mechanisms of NO formation and destruction due to the addition of hydrogen. It is well established that the temperature is vital for the evolution of NO, especially that some NO mechanisms are strongly dependent on temperature. For the present study, the in-furnace and wall temperatures of the CFD and experiment are compared firstly, and then the NO mechanism calculation is carried out. In Fig. 3a–c the comparison of the experimental and numerical in-furnace temperature, obtained along the z axis at x = 0 mm and y = 0 mm, 50 mm and 100 mm of Case 2 is shown. It is clear that the CFD results agree well with the measured average temperatures. Fig. 3d shows a comparison of the experimental and numerical furnace wall temperature, obtained along the z axis at x = 0 mm and y = 140 mm. The furnace wall temperature in the CFD models is set by using the user-defined-function of FLUENT [53] and it is consistent with those measured experimentally. Therefore, the thermal field of the CFD result is validated with the experiments and provides confidence in performing analyses of the NO field.

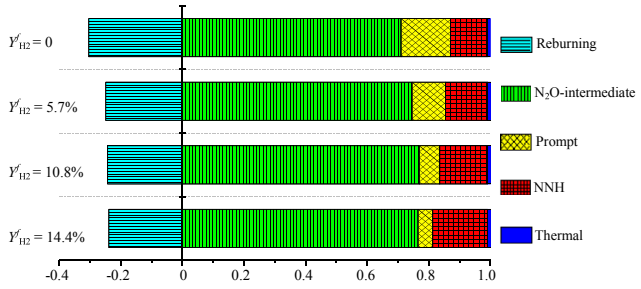

Fig. 4 – Calculated relative importance of NO emissions via thermal, prompt, N_2O-intermediate, and reburning routes at the furnace exit (Cases 1–4).

Fig. 4 depicts calculated NO emissions via thermal, prompt, N_2O-intermediate, and reburning routes at the furnace exit. The calculation method is introduced in sub-section CFD calculations . It is evident that the N_2O-intermediate route dominates the NO formation in all the cases, with its contribution growing slightly as $Y^f_{H_2}$ is increased. When $Y^f_{H_2} = 0\%$ or burning natural gas, the N_2O-intermediate mechanism accounts for 71% of the total NO formation. The rest of NO is formed from the prompt and NNH routes. The NO-reburning reaction is strong and reduces the NO formation by about 30%. This is consistent with those of Li et al. [45,46] who used different burner configurations and fuel mixture from the present. Those authors found that the NO mainly comes from the N_2O-intermediate route, regardless of the hydrocarbon fuel type and oxidant type [45] and premixing pattern [46]. Therefore, it is concluded that, when $\Phi \leq 0.8$, the N_2O-intermediate route at these temperatures is always the dominant NO formation mechanism under MILD combustion, regardless

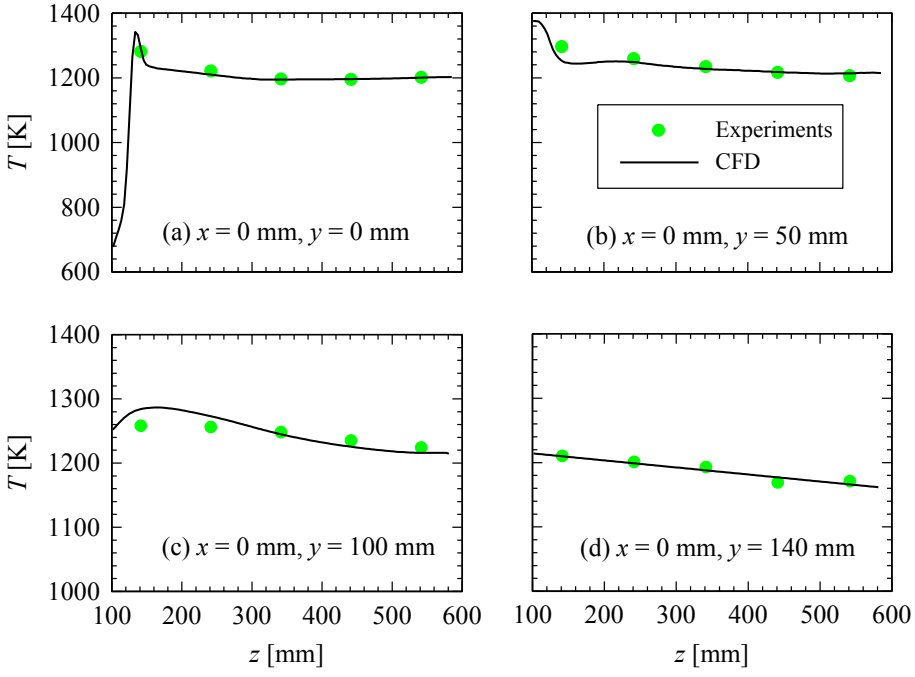

Fig. 3 – Comparison of the experimental and numerical furnace temperature profiles along the z axis at x = 0 mm and y = 0 mm, 50 mm, 100 mm and 140 mm (Case 2).

of the hydrocarbon fuel type, the hydrogen addition, the oxidant type, and burner configuration.

As $Y^f_{H_2}$ is increased from 0 to 5.7%, the N_2O-intermediate yields more NO formation and the NO reduction from NO-reburning is reduced. So, the measured NO emission is increased (see Fig. 2). However, as $Y^f_{H_2}$ is further increased from 5.7% to 14.4%, NO formation from the prompt route is decreased while that from the NNH route is increased. As a result, the total NO emission changes insignificantly as measured in experiments (Fig. 2). Fig. 4 also reveals that unsurprisingly at these temperatures, the thermal NO mechanism can be ignored for all the MILD cases, which differs significantly from the conventional combustion. To more deeply understand the NO mechanism under the MILD combustion of CH_4/H_2, detailed chemical kinetic calculations using WSR model are carried out to examine the effects of hydrogen addition, reactor temperature, mass fraction of oxygen and equivalence ratio, and the results are presented below.

Chemical kinetics calculation results

Effects of H_2 addition

Fig. 5 displays the reaction path diagram for reactive nitrogen conversion in the MILD combustion of CH_4 and CH_4/H_2 mixtures. N_2 convert to NO mainly through the $N_2 \rightarrow N_2O \rightarrow NO$, $N_2 \rightarrow NNH \rightarrow NO$, $N_2 \rightarrow HCN \rightarrow NCO \rightarrow NO$ and $N_2 \rightarrow N \rightarrow NO$ routes. The $N_2 \rightarrow N_2O \rightarrow NO$ pathway corresponds to the N_2O-intermediate mechanism. The $N_2 \rightarrow NNH \rightarrow NO$ trail is the NNH mechanism while the prompt NO route is $N_2 \rightarrow HCN \rightarrow NCO \rightarrow NO$. Therefore, it is consistent with the CFD results of the above sub-section, the reaction path diagram analysis also shows that N_2O-intermediate, NNH and prompt routes are the vital reactions in producing NO under the MILD condition. Moreover, the NO is reduced through the $NO \rightarrow HNO$, $NO \rightarrow HCNO$, $NO \rightarrow HNCO$ and $NO \rightarrow HCN$ pathways. This indicates that the NO-reburning is important under the MILD condition, reducing the NO formation mainly through reactions $CH_2 + NO \rightleftharpoons H + HNCO$, $H + NO + M \rightleftharpoons HNO + M$, $CH_2 + NO \rightleftharpoons H + HCNO$, and $CH_2 + NO \rightleftharpoons OH + HCN$. Furthermore, the mutual conversion between NO and NO_2 is significant. The NO/NO_2 conversion reactions become strong in low temperatures [71]. However, for conventional combustion, no NO_2 is formed in high-temperature regions because NO_2 destruction reactions are extremely strong at high temperatures [71].

The results for Cases 5–7 of the first-order sensitivity analysis for NO are presented in Fig. 6. The first two sensitivity reactions for the NO reduction are $N_2O + H \rightleftharpoons N_2 + OH$ and $H + O_2 + N_2 \rightleftharpoons HO_2 + N_2$. The sensitivity coefficients for these reactions are negative, indicating that increasing the reaction rate will lead to more NO reduction. HO_2 is largely formed under the low temperature regime of MILD condition through this reaction and thus significant NO is converted to NO_2 via reaction $NO + HO_2 \rightleftharpoons NO_2 + OH$. The first three maximum sensitivity reactions for the NO formation are $N_2O + H \rightleftharpoons NH + NO$, $N_2O + O \rightleftharpoons 2NO$ and $N_2O (+M) \rightleftharpoons N_2 + O (+M)$. The sensitivity coefficients of these reactions are positive which indicates that increasing the rate of these reactions will lead to more NO production. Reactions $N_2O + H \rightleftharpoons NH + NO$ and $N_2O + O \rightleftharpoons 2NO$ correspond to the N_2O-intermediate route. Therefore, the N_2O-intermediate reaction is the most important route for the NO production under these MILD condition. The NNH route ($NNH + O \rightleftharpoons NH + NO$) is significant as well but it is less important than the N_2O-intermediate route. Fig. 6 further

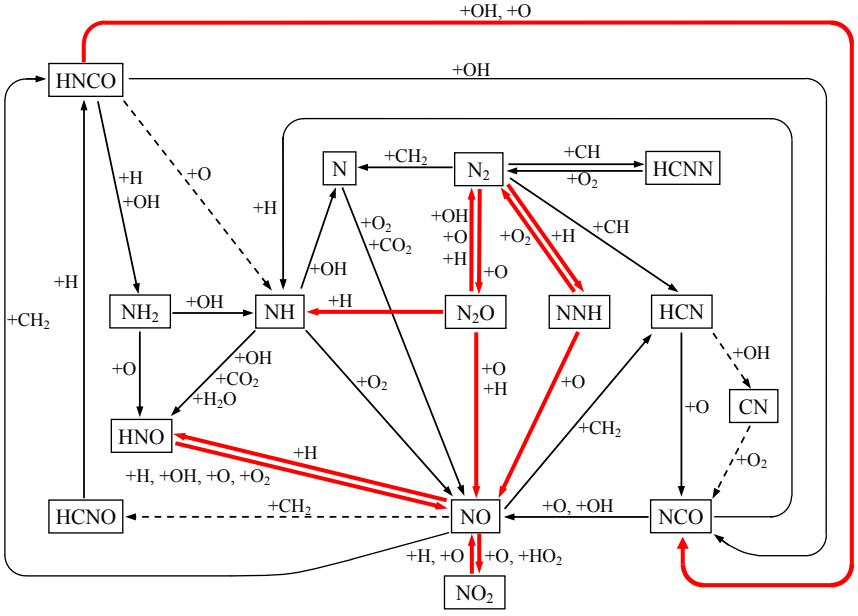

Fig. 5 – Reaction path diagram for reactive nitrogen conversion in the MILD combustion of CH_4 and CH_4/H_2 mixtures. The dashed lines denote pathways only important in the MILD combustion of CH_4 (Case 5). The red lines denote those pathways becoming more important in the MILD combustion of CH_4/H_2 mixtures (Cases 6–7). (For interpretation of the references to color in this figure legend, the reader is referred to the web version of this article.)

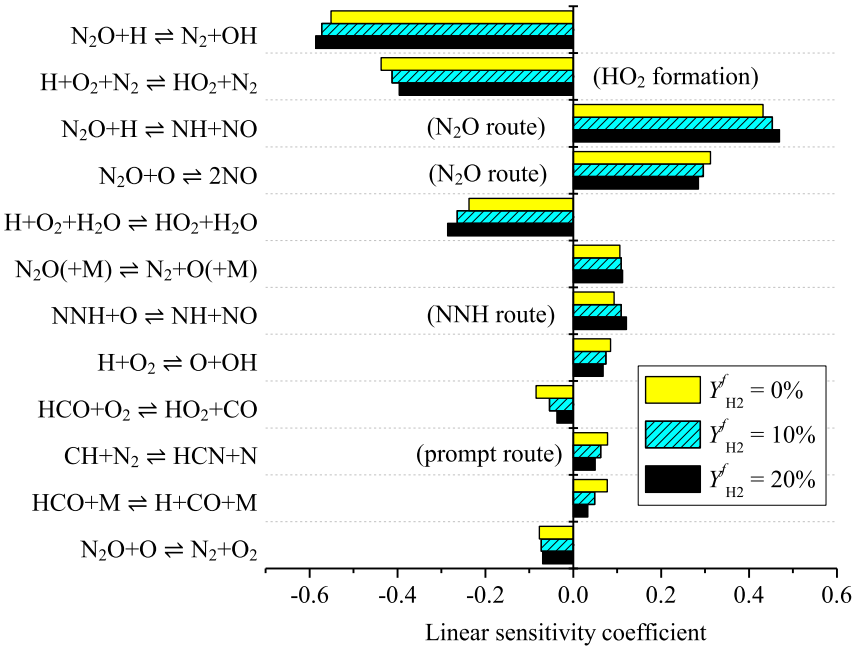

Fig. 6 – Results of the first-order NO sensitivity analysis for Cases 5–7.

suggests that the prompt route produces some NO via its key step $CH + N_2 \rightleftharpoons HCN + N$. The prompt route is weaker than the N_2O and NNH routes.

Moreover, as more hydrogen is added, the sensitivity coefficient of reaction $NNH + O \rightleftharpoons NH + NO$ is increased because more NNH radical is formed via reaction $N_2 + H\ (+M) \rightleftharpoons NNH\ (+M)$. Consequently, thus more NO is produced from the NNH route with hydrogen addition. However, as more hydrogen is added, the sensitivity coefficients of reaction $CH + N_2 \rightleftharpoons HCN + N$ is decreased due to the consumption of CH through reaction $CH + H_2 \rightleftharpoons H + CH_2$. Therefore, NO formed from the prompt route is decreased with the hydrogen addition. This WSR result is consistent with the CFD result of Fig. 4.

Effects of reactor temperature

Fig. 7 displays the first-order sensitivity analysis for NO for Cases 8–10. Clearly, the N_2O route ($N_2O + H \rightleftharpoons NH + NO$ and

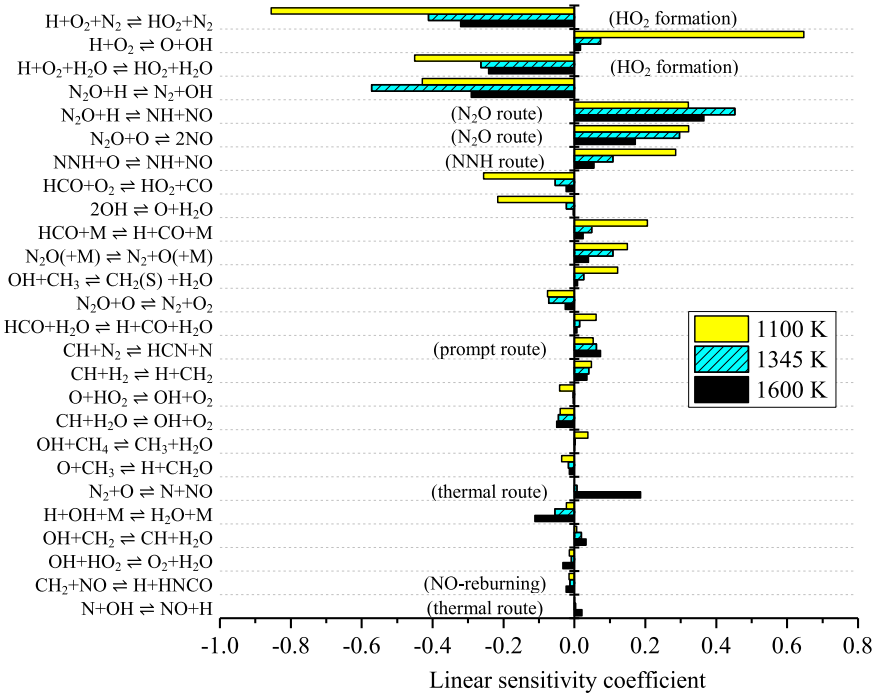

Fig. 7 – First-order sensitivity analysis for NO for Cases 8–10.

$N_2O + O \rightleftharpoons 2NO$) is dominant, regardless of the reactor temperature. The NNH ($NNH + O \rightleftharpoons NH + NO$) and prompt ($CH + N_2 \rightleftharpoons HCN + N$) routes are less important but also play their role in production NO. The NO-reburning reaction $CH_2 + NO \rightleftharpoons H + HNCO$ reduces NO production. As the reactor temperature is increased from 1100 K to 1600 K, the importance of the NNH route decreases, while those of prompt and thermal routes increase. Importantly, as T_{WSR} is reduced from 1600 K to 1100 K, the sensitivity of reactions $H + O_2 + N_2 \rightleftharpoons HO_2 + N_2$ and $H + O_2 + H_2O \rightleftharpoons HO_2 + H_2O$ decreases. HO_2 is formed through these reactions and thus more NO is converted to NO_2 through reaction $NO + HO_2 \rightleftharpoons NO_2 + OH$. Consequently, the relative importance of NO_2 to the total NO_x is increased under low temperature condition found in MILD condition.

Effects of the mass fraction of oxygen

Fig. 8 illustrates the first-order sensitivity analysis for NO for Cases 11–13. Clearly, as the mass fraction of oxygen ($Y^o_{O_2}$) is increased, the importance of the N_2O route increases because more NO is produced from the reaction $N_2O + O \rightleftharpoons 2NO$. However, the importance of the NNH route decreases because less NNH radicals are produced with the oxygen addition via reactions $N_2 + H (+M) \rightleftharpoons NNH (+M)$. Moreover, the sensitivity of the prompt mechanism also reduces because less CH radicals are formed as the reaction condition becomes fuel lean.

Effects of the equivalence ratio

The first-order sensitivity analysis for NO for Cases 14–16 is shown in Fig. 9. For $\Phi = 0.5$, the NO is mainly produced from the N_2O-intermediate route through reactions $N_2O + O \rightleftharpoons 2NO$. Reactions $H + O_2 + N_2 \rightleftharpoons HO_2 + N_2$ and $H + O_2 + H_2O \rightleftharpoons HO_2 + H_2O$ have highly sensitivity for reducing NO via the reaction $NO + HO_2 \rightleftharpoons NO_2 + OH$. For $\Phi = 1$, the NO is mostly formed from the prompt mechanism (via the reaction $CH + N_2 \rightleftharpoons HCN + N$) while the NNH route ($NNH + O \rightleftharpoons NH + NO$) is also notable. The NO-reburning reaction ($CH_2 + NO \rightleftharpoons H + HNCO$) becomes important at $\Phi = 1$. For $\Phi = 1.5$, both the prompt and NO-reburning routes ($CH_2 + NO \rightleftharpoons H + HNCO$ and $HCCO + NO \rightleftharpoons HCNO + CO$) become extremely stronger.

Quantitative analysis of the NO mechanism

Relative importance of the NO mechanism through WSR modeling

The above analysis on the NO formation and destruction mechanisms is conducted using the WSR model with the GRI-Mech 2.11 mechanism. The sensitivity of the different reactions that contribute to the NO production and destruction is investigated, while the contribution of each NO mechanism to total NO formation is not obtained. This is quantitatively investigated in this section.

It is worth mentioning that reactions of each NO mechanism are complicated and coupled with each other. Results may not be true if different NO pathway are decouple [72]. For the present investigation, the relative importance of the thermal, prompt, N_2O-intermediate, NNH and NO-reburning routes is obtained by performing calculations with each mechanism at a time. For each calculation of a particular mechanism, relevant reactions are included to avoid omitting some coupled reactions. Table 4 shows main reactions of different NO routes for the present calculation.

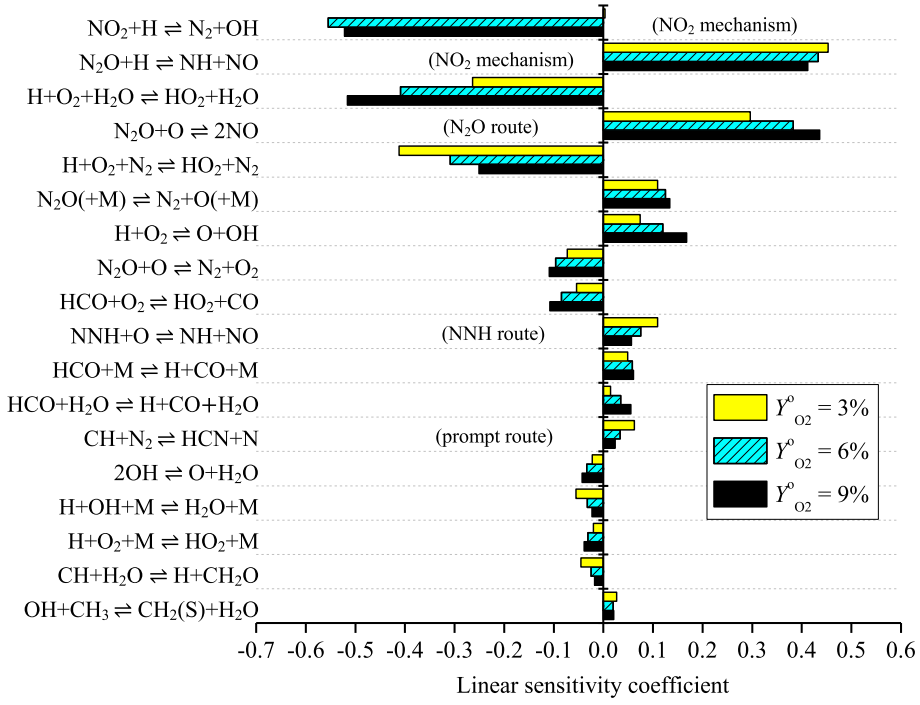

Fig. 8 – First-order sensitivity analysis for NO for Cases 11–13.

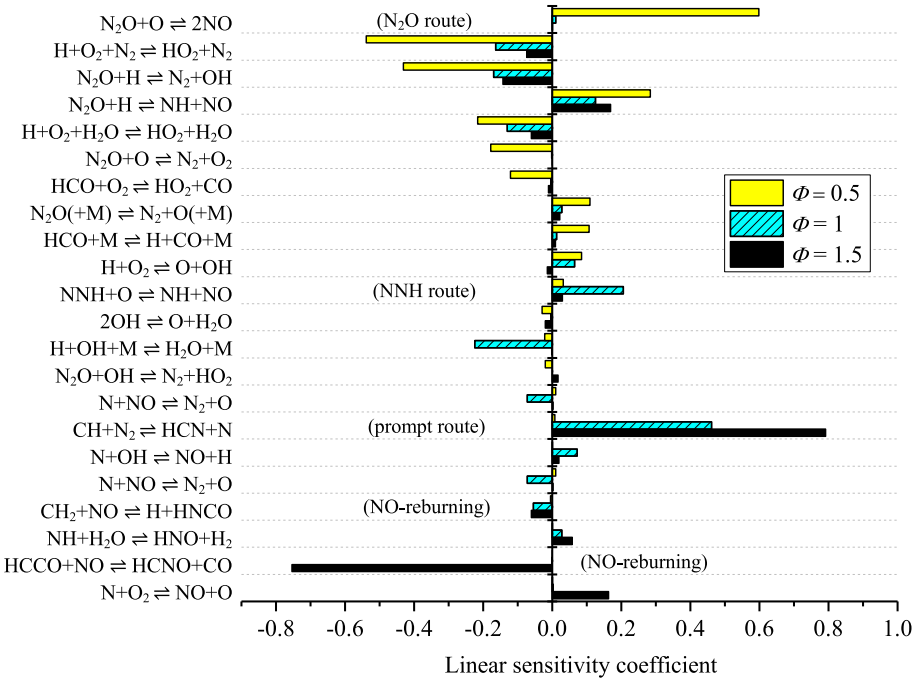

Fig. 9 – First-order sensitivity analysis for NO for Cases 14–16.

For the thermal route, the extended Zeldovich mechanism is considered. For the prompt route, CH and CH_2 radicals react with molecular nitrogen to from HCN through reactions $CH + N_2 \rightleftharpoons HCN + N$ and $CH_2 + N_2 \rightleftharpoons HCN + NH$. HCN and N convert to NO via series of intermediate reactions of Table 4 [73]. For the N_2O-intermediate route, N_2 converted to N_2O and then NO via reactions $N_2 + O + (+M) \rightleftharpoons N_2O\ (+M)$, $H + N_2O \rightleftharpoons NO + NH$, $O + N_2O \rightleftharpoons 2NO$ and other series of

Table 4 – Main reactions of different NO routes.

NO formation	Main reactions		
Thermal	$N + NO \rightleftharpoons N_2 + O$	$N + O_2 \rightleftharpoons NO + O$	$N + OH \rightleftharpoons NO + H$
Prompt	$N + OH \rightleftharpoons NO + H$	$NH + H \rightleftharpoons N + H_2$	$CN + O_2 \rightleftharpoons NCO + O$
	$NCO + O \rightleftharpoons NO + CO$	$NCO + H \rightleftharpoons NH + CO$	$HCN + M \rightleftharpoons CN + H + M$
	$HCN + O \rightleftharpoons NCO + H$	$HCN \rightleftharpoons CN + H$	$C + N_2 \rightleftharpoons CN + N$
	$CH + N_2 \rightleftharpoons HCN + N$	$CH_2 + N_2 \rightleftharpoons HCN + NH$	$CH_2(S) + N_2 \rightleftharpoons NH + HCN$
N_2O-intermediate	$N_2O + O \rightleftharpoons N_2 + O_2$	$N_2O + O \rightleftharpoons 2NO$	$N_2O + H \rightleftharpoons N_2 + OH$
	$N_2O + OH \rightleftharpoons N_2 + HO_2$	$N_2O\ (+M) \rightleftharpoons N_2 + O\ (+M)$	$NH + O \rightleftharpoons NO + H$
	$NH + NO \rightleftharpoons N_2O + H$	$NCO + O \rightleftharpoons NO + CO$	$NCO + OH \rightleftharpoons NO + H + CO$
	$NCO + O_2 \rightleftharpoons NO + CO_2$		
NNH Route	$NH + O \rightleftharpoons NO + H$	$NH + H \rightleftharpoons N + H_2$	$NH + OH \rightleftharpoons HNO + H$
	$NH + OH \rightleftharpoons N + H_2O$	$NH + O_2 \rightleftharpoons HNO + O$	$NH + O_2 \rightleftharpoons NO + OH$
	$NH + N \rightleftharpoons N_2 + H$	$NH + H_2O \rightleftharpoons HNO + H_2$	$NH + NO \rightleftharpoons N_2 + OH$
	$NH + NO \rightleftharpoons N_2O + H$	$NNH \rightleftharpoons N_2 + H$	$NNH + M \rightleftharpoons N_2 + H + M$
	$NNH + O_2 \rightleftharpoons HO_2 + N_2$	$NNH + O \rightleftharpoons OH + N_2$	$NNH + O \rightleftharpoons NH + NO$
	$NNH + H \rightleftharpoons H_2 + N_2$	$NNH + OH \rightleftharpoons H_2O + N_2$	$NNH + CH_3 \rightleftharpoons CH_4 + N_2$
	$H + NO + M \rightleftharpoons HNO + M$	$HNO + O \rightleftharpoons NO + OH$	$HNO + H \rightleftharpoons H_2 + NO$
	$HNO + OH \rightleftharpoons NO + H_2O$	$HNO + O_2 \rightleftharpoons HO_2 + NO$	
NO-reburning	$N_2O + H \rightleftharpoons N_2 + OH$	$NH + N \rightleftharpoons N_2 + H$	$NH + NO \rightleftharpoons N_2 + OH$
	$NH + NO \rightleftharpoons N_2O + H$	$CN + OH \rightleftharpoons NCO + H$	$CN + O_2 \rightleftharpoons NCO + O$
	$NCO + H \rightleftharpoons NH + CO$	$NCO + NO \rightleftharpoons N_2 + CO_2$	$HCN + O \rightleftharpoons NCO + H$
	$HCN + O \rightleftharpoons NH + CO$	$HCN + O \rightleftharpoons CN + OH$	$HCN + OH \rightleftharpoons HOCN + H$
	$HCN + OH \rightleftharpoons HNCO + H$	$HCN + OH \rightleftharpoons NH_2 + CO$	$C + NO \rightleftharpoons CN + O$
	$C + NO \rightleftharpoons CO + N$	$CH + NO \rightleftharpoons HCN + O$	$CH + NO \rightleftharpoons H + NCO$
	$CH + NO \rightleftharpoons N + HCO$	$CH_2 + NO \rightleftharpoons H + HNCO$	$CH_2 + NO \rightleftharpoons OH + HCN$
	$CH_2 + NO \rightleftharpoons H + HCNO$	$CH_2(S) + NO \rightleftharpoons H + HNCO$	$CH_2(S) + NO \rightleftharpoons OH + HCN$
	$CH_2(S) + NO \rightleftharpoons H + HCNO$	$CH_3 + NO \rightleftharpoons HCN + H_2O$	$CH_3 + NO \rightleftharpoons H_2CN + OH$
	$HCCO + NO \rightleftharpoons HCNO + CO$		

intermediate reactions [65]. For the NNH route, NO is produced through reactions $N_2 + H (+M) \rightleftharpoons NNH (+M)$, $NNH + O \rightleftharpoons NO + NH$ and other series of intermediate reactions [73]. For the NO-reburning mechanism, Dagaut et al. [74] found that NO-reduction by the CH_4/H_2 fuel occurs via $HCCO + NO \rightleftharpoons HCN + CO_2$, $HCCO + NO \rightleftharpoons HCNO + CO$, $HCNO + H \rightleftharpoons HCN + OH$, $HCN + O \rightleftharpoons NH + CO$, $HCN + O \rightleftharpoons CN + OH$, $HCN + O \rightleftharpoons NCO + H$, $HCN + OH \rightleftharpoons HOCN + H$, $HCN + OH \rightleftharpoons HNCO + H$, $HCN + OH \rightleftharpoons NH_2 + CO$, $CN + O_2 \rightleftharpoons NCO + O$, $CN + OH \rightleftharpoons NCO + H$, $NCO + H \rightleftharpoons NH + CO$, $NH + NO \rightleftharpoons N_2O + H$ and $N_2O + H \rightleftharpoons N_2 + OH$. Other intermediate reactions of NO-reburning mechanism are also considered in Table 4. The calculated relative importance of NO formations and reductions via thermal, prompt, N_2O-intermediate, NNH, and reburning routes of the WSR model of Cases 5–16 is displayed in Fig. 10.

Clearly from Fig. 10, for $\Phi \leq 0.8$ (Cases 5–14), the N_2O-intermediate route plays the most significant role in the total NO formation, regardless of the hydrogen addition ($Y^f_{H_2}$ = 0%–20%), initial mass fraction of oxygen in oxidant ($Y^o_{O_2}$ = 3%–9%) and reactor temperature (T_{WSR} = 1100 K–1600 K). The N_2O-intermediate contributes 60%–90% of the total NO formation. The prompt and NNH routes are also important. The NO-reburning reaction is strong which reduces 30%–50% of the total NO formation.

For Cases 5–7, with the addition of hydrogen, the importance of the NNH routes increases. However, the prompt and NO-reburning reactions significantly become weak with the hydrogen addition. This result is consistent with CFD results of Fig. 4.

For Cases 8–10, effects of the reactor temperature (T_{WSR}) on the NO mechanism is obtained. Clearly, the N_2O-intermediate route controls the total NO formation. However, as T_{WSR} is increased from 1100 K to 1600 K, the relative importance of the N_2O-intermediate route to the total NO formation decreases from 93% to 62%, while that of the thermal route increases from 0.03% to 24%. For T_{WSR} = 1345 K, the relative importance of NNH and NO-reburning routes are higher than that of T_{WSR} = 1100 K or 1600 K.

For Cases 11–13, effects of initial mass fraction of oxygen ($Y^o_{O_2}$) on the NO mechanism is investigated. Obviously, the N_2O-intermediate mechanism also controls the total NO production, regardless of $Y^o_{O_2}$. As $Y^o_{O_2}$ is increased from 3% to 9%, the relative importance of the N_2O-intermediate increases, while that of prompt and NNH routes decrease.

For Cases 14–16, effects of equivalence ratio (Φ) on the NO mechanism is examined. For Case 14, $\Phi = 0.5$, the N_2O-intermediate route is extremely strong and it accounts for 95% of the total NO formation. The prompt and NNH routes are unimportant at $\Phi = 0.5$. However, for Cases 15 and 16, $\Phi = 1$ and 1.5, respectively. The prompt route is so strong that it contributes more than 55% of the total NO formation. Especially, the prompt route accounts for 90% of the total NO formation at $\Phi = 1.5$. Moreover, the NO-reburning reaction reduces approximately 20% of the total NO formation at $\Phi = 0.5$. The NO-reburning reaction significantly becomes stronger as Φ increases from 0.5 to 1.5.

Effects of the chemical kinetic scheme

Although considerable investigators found that GRI-Mech 2.11 is better than GRI-Mech 3.0 in the NO_x modeling [66–69], some studies also found that GRI-Mech 3.0 is suitable for the MILD combustion modeling [31,34,38,39,43,75,76]. In this section, we examine the NO routes using GRI-Mech 3.0 to investigate the effect of the kinetic scheme. The relative importance of each route is obtained by calculation with one mechanism at a time and the mechanism of each route is shown in Table 4. Fig. 11 shows the calculated NO formation and reduction via

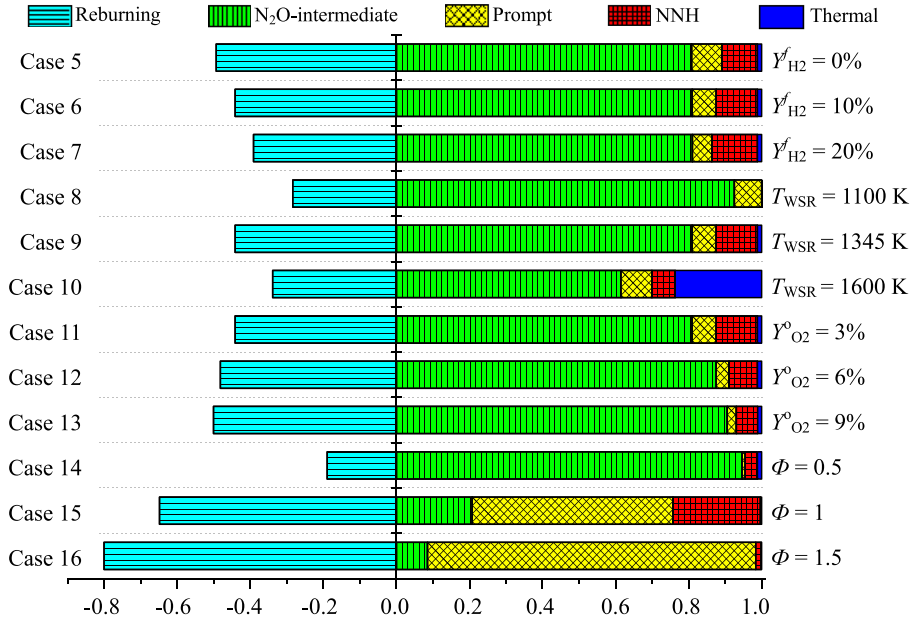

Fig. 10 – Calculated relative importance of NO formations and reductions via thermal, prompt, N_2O-intermediate, NNH, and reburning routes of the WSR model using GRI-Mech 2.11 mechanism.

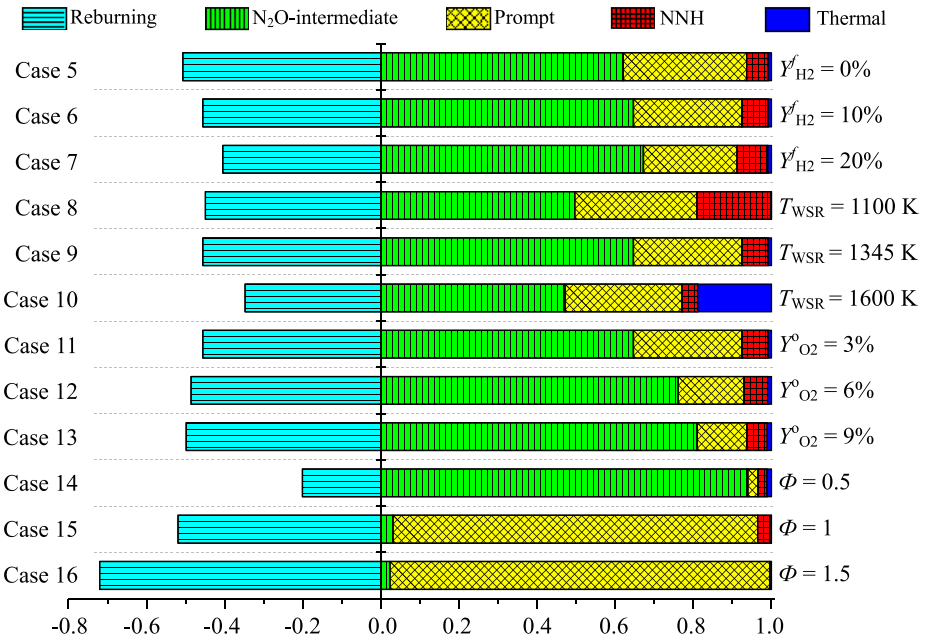

Fig. 11 – Calculated relative importance of NO formations and reductions via thermal, prompt, N_2O-intermediate, NNH, and reburning routes of the WSR model using GRI-Mech 3.0 mechanism.

thermal, prompt, N_2O-intermediate, NNH, and reburning routes of the WSR model of Cases 5–13 using GRI-Mech 3.0.

Comparing with Fig. 10, it is discovered from Fig. 11 that the similar result is obtained by using GRI-Mech 3.0, while the relative importance of the prompt route increases. There is indeed difference of the prompt route between two GRI mechanisms. Lee et al. [66] found that GRI-Mech 2.11 gives reasonably good agreement with the measured NO for the CH_4/H_2 bluff body flame but it under-predicts NO levels in the fuel rich region. They also pointed out that GRI-Mech 3.0 gives higher prompt NO formation compared to GRI-Mech 2.11. Barlow et al. [67] found that GRI-Mech 2.11 provides decent agreement with measured NO levels in lean and near-stoichiometric conditions, but it under-predicts NO levels in fuel-rich conditions of the methane and air flame. They also noticed that GRI-Mech 3.0 significantly over predicts the peak NO levels for the $\Phi = 3.17$ and 2.17 flames, but it yields relatively good agreement with measurements in the $\Phi = 1.8$ flame. They agreed that there is some difference of the prompt mechanism between GRI-Mech 2.11 and 3.0. Kim et al. [68,69] discovered that the GRI-Mech 3.0 significantly over-predicts the NO formation except in a fuel-rich condition, while the GRI-Mech 2.11 gives acceptable results on the overall. In GRI-Mech 3.0 the rate coefficient of reaction $CH + N_2 \rightleftharpoons N + HCN$ is much higher than that in GRI-Mech 2.11. A higher pre-exponential factor for this prompt route is the major reason for the over-predicted NO.

Conclusions

The present study has experimentally and numerically investigated the effect of hydrogen addition on the characteristics of MILD combustion and the NO mechanism. When the MILD combustion of NG and NG/H_2 fuels is achieved in the experiments, quite a uniform temperature distribution and very low emissions of NO_x are obtained. The NO formation and reduction mechanisms under the MILD condition of CH_4/H_2 mixtures are examined with detailed chemical kinetics model. The main conclusions are summarized below:

(1) In the experiments, with the addition of hydrogen, although the furnace temperature is increased, the location of the high temperature zone does not change. This high temperature region is located at the V-shaped junction of the upward fresh fuel jet and downward recirculated air jet. Moreover, as the mass fraction of hydrogen in fuel ($Y^f_{H_2}$) is increased from 5.7% to 14.4%, both the furnace average temperature and extracted heat are increased, but the NO_x emission remains unchanged.

(2) From the CFD and WSR simulations it is found that, for lean conditions ($\Phi \leq 0.8$), the N_2O-intermediate route is the most important mechanism for producing NO under MILD combustion of CH_4/H_2 (taking 60%–90% of the total NO formation), regardless of the hydrogen addition ($Y^f_{H_2}$ = 0%–20%), initial mass fraction of oxygen in oxidant ($Y^o_{O_2}$ = 3%–9%), reactor temperature (T_{WSR} = 1100 K–1600 K) and burner configuration. The prompt and NNH routes also produce NO formation but they are less important. The NO-reburning reaction is significant and reduces 30%–50% of the total NO formed.

(3) For the MILD combustion at $\Phi = 0.8$, as hydrogen is added to the fuel, the NO production from NNH route increases while that from the prompt route decreases. However, the addition of hydrogen does not change noticeably the NO production from the N_2O-

intermediate route. As a result, as $Y^f_{H_2}$ is increased from 5.7% to 14.4%, the measured NO emission changes little.

(4) For the MILD combustion at $\Phi = 0.8$, as the reactor temperature (T_{WSR}) is increased from 1100 K to 1600 K, the N_2O-intermediate route remains dominant but its importance reduces and also the thermal route becomes more important. The conversion from NO to NO_2 is stronger at low temperatures and thus the relative importance of NO_2 to the total NO_x emission increases as the reactor temperature decreases.

(5) For the MILD combustion at $\Phi = 0.8$, as the initial mass fraction of oxygen is increased from 3% to 9%, the N_2O-intermediate route increases its contribution in the NO formation whereas those of prompt and NNH routes decrease.

(6) For the MILD combustion at $\Phi = 0.5$, the N_2O-intermediate route is extremely important and its contribution accounts for 94% of the total NO formation. However, as Φ is increased, the N_2O-intermediate route weakens dramatically while the prompt and NO-reburning routes become dominant.

(7) The present finding is insensitive to the kinetic scheme GRI-Mech 2.11 or GRI-Mech 3.0, although the latter overpredicts the NO formation through the prompt route.

Acknowledgments

This work is supported by the National Natural Science Foundation of China (No. 51276002, No. 51406001), China Postdoctoral Science Foundation (2014M550011) and the Centre for Global New Energy Strategy Studies of Peking University (No. 201408).

REFERENCES

[1] Giakoumis EG, Rakopoulos CD, Dimaratos AM, Rakopoulos DC. Exhaust emissions of diesel engines operating under transient conditions with biodiesel fuel blends. Prog Energy Combust Sci 2012;38(5):691–715.

[2] Chen Z, Dai P, Chen S. A model for the laminar flame speed of binary fuel blends and its application to methane/hydrogen mixtures. Int J Hydrogen Energy 2012;37(13):10390–6.

[3] Chen S, Li J, Han H, Liu Z, Zheng C. Effects of hydrogen addition on entropy generation in ultra-lean counter-flow methane–air premixed combustion. Int J Hydrogen Energy 2010;35(8):3891–902.

[4] Wang J, Huang Z, Zheng J, Miao H. Effect of partially premixed and hydrogen addition on natural Gas direct-injection lean combustion. Int J Hydrogen Energy 2009;34(22):9239–47.

[5] Chen Z. Effects of hydrogen addition on the propagation of spherical methane/air flames: a computational study. Int J Hydrogen Energy 2009;34(15):6558–67.

[6] Shrestha SOB, Karim GA. Hydrogen as an additive to methane for spark ignition engine applications. Int J Hydrogen Energy 1999;24(6):577–86.

[7] Bauer CG, Forest TW. Effect of hydrogen addition on the performance of methane-fueled vehicles. Part I: effect on SI engine performance. Int J Hydrogen Energy 2001;26(1):55–70.

[8] Cavaliere A, de Joannon M. Mild combustion. Prog Energy Combust Sci 2004;38(4):329–66.

[9] Li P, Mi J, Dally BB, Wang F, Wang L, Liu Z, et al. Progress and recent trend in MILD combustion. Sci China Ser E-Technol Sci 2011;54(2):255–69.

[10] Tsuji H, Gupta AK, Hasegawa T, Katsuki M, Kishimoto K, Morita M. High temperature air combustion: from energy conservation to pollution reduction. Boca Raton, FL: CRC Press; 2003.

[11] Wünning JA, Wünning JG. Flameless oxidation to reduce thermal no-formation. Prog Energy Combust Sci 1997;23(1):81–94.

[12] Wang F, Li P, Mei Z, Zhang J, Mi J. Combustion of $CH_4/O_2/N_2$ in a well stirred reactor. Energy 2014;72(1):42–253.

[13] Mei Z, Li P, Wang F, Zhang J, Mi J. Influences of reactant injection velocities on moderate or intense low-oxygen dilution coal combustion. Energy Fuels 2014;28(1):369–84.

[14] Mi J, Li P, Zheng C. Impact of injection conditions on flame characteristics from a parallel multi-jet burner. Energy 2011;36(11):6583–95.

[15] Weber R, Smart JP, vd Kamp W. On the (MILD) combustion of gaseous, liquid, and solid fuels in high temperature preheated air. Proc Combust Inst 2005;30(2):2623–9.

[16] Arghode VK, Gupta AK, Bryden KM. High intensity colorless distributed combustion for ultra low emissions and enhanced performance. Appl Energy 2012;92:822–30.

[17] Galbiati MA, Cavigiolo A, Effuggi A, Gelosa D, Rota R. Mild combustion for fuel-NO_x reduction. Combust Sci Technol 2004;176(7):1035–54.

[18] de Joannon M, Matarazzo A, Sabla P, Cavaliere A. Mild combustion in homogeneous charge diffusion ignition (HCDI) regime. Proc Combust Inst 2007;31(2):3409–16.

[19] Veríssimo AS, Rocha AMA, Costa M. Experimental study on the influence of the thermal input on the reaction zone under flameless oxidation conditions. Fuel Process Technol 2013;106:423–8.

[20] Reddy MV, Sawant D, Trivedi D, Kumar S. Studies on a liquid fuel based two stage flameless combustor. Proc Combust Inst 2013;34(2):3319–26.

[21] Yang W, Blasiak W. Flame entrainments induced by a turbulent reacting jet using high-temperature and oxygen-deficient oxidizers. Energy Fuels 2005;19(4):1473–83.

[22] Stadler H, Christ D, Habermehl M, Heil P, Kellermann A, Ohliger A, et al. Experimental investigation of NO_x emissions in oxycoal combustion. Fuel 2011;90(4):1604–11.

[23] Oldenhof E, Tummers MJ, van Veen EH, Roekaerts DJEM. Conditional flow field statistics of jet-in-hot-coflow flames. Combust Flame 2013;160(8):1428–40.

[24] Mardani A, Tabejamaat S, Hassanpour S. Numerical study of CO and CO_2 formation in CH_4/H_2 blended flame under MILD condition. Combust Flame 2013;160(9):1636–49.

[25] Ihme M, See YC. LES flamelet modeling of a three-stream MILD combustor: analysis of flame sensitivity to scalar inflow conditions. Proc Combust Inst 2011;33(1):1309–17.

[26] Minamoto Y, Swaminathan N. Scalar gradient behaviour in MILD combustion. Combust Flame 2014;161(4):1063–75.

[27] Chen S, Zheng C. Counterflow diffusion flame of hydrogen-enriched biogas under mild oxy-fuel condition. Int J Hydrogen Energy 2011;36(23):15403–13.

[28] Chen S, Mi J, Liu H, Zheng C. First and second thermodynamic-law analyses of hydrogen-air counter-flow diffusion combustion in various combustion modes. Int J Hydrogen Energy 2012;37(6):5234–45.

[29] Derudi M, Villani A, Rota R. Sustainability of mild combustion of hydrogen-containing hybrid fuels. Proc Combust Inst 2007;31(2):3393–400.
[30] Derudi M, Villani A, Rota R. Mild combustion of industrial hydrogen-containing byproducts. Ind Eng Chem Res 2007;46(21):6806–11.
[31] Parente A, Galletti C, Tognotti L. Effect of the combustion model and kinetic mechanism on the MILD combustion in an industrial burner fed with hydrogen enriched fuels. Int J Hydrogen Energy 2008;33(24):7553–64.
[32] Parente A, Galletti C, Tognotti L. A simplified approach for predicting NO formation in MILD combustion of CH_4–H_2 mixtures. Proc Combust Inst 2011;33(2):3343–50.
[33] Arghode VK, Gupta AK. Hydrogen addition effects on methane–air colorless distributed combustion flames. Int J Hydrogen Energy 2011;36(10):6292–302.
[34] Galletti C, Parente A, Derudi M, Rota R, Tognotti L. Numerical and experimental analysis of NO emissions from a lab-scale burner fed with hydrogen-enriched fuels and operating in MILD combustion. Int J Hydrogen Energy 2009;34(19):8339–51.
[35] Ayoub M, Rottier C, Carpentier S, Villermaux C, Boukhalfa AM, Honoré D. An experimental study of mild flameless combustion of methane/hydrogen mixtures. Int J Hydrogen Energy 2012;37(8):6912–21.
[36] Yu Y, Gaofeng W, Qizhao L, Chengbiao M, Xianjun X. Flameless combustion for hydrogen containing fuels. Int J Hydrogen Energy 2010;35(7):2694–7.
[37] Dally BB, Karpetis AN, Barlow RS. Structure of turbulent non-premixed jet flames in a diluted hot coflow. Proc Combust Inst 2002;29(1):1147–54.
[38] Wang F, Mi J, Li P, Zheng C. Diffusion flame of a CH_4/H_2 jet in hot low-oxygen coflow. Int J Hydrogen Energy 2011;36(15):9267–77.
[39] Medwell PR, Dally BB. Effect of fuel composition on jet flames in a heated and diluted oxidant stream. Combust Flame 2012;159(10):3138–45.
[40] Mardani A, Tabejamaat S. Effect of hydrogen on hydrogen–methane turbulent non-premixed flame under MILD condition. Int J Hydrogen Energy 2010;35(20):11324–31.
[41] Mardani A, Tabejamaat S. NO_x formation in H_2–CH_4 blended flame under MILD conditions. Combust Sci Technol 2012;184(7–8):995–1010.
[42] Gao X, Duan F, Lim SC, Yip MS. NO_x formation in hydrogen–methane turbulent diffusion flame under the moderate or intense low-oxygen dilution conditions. Energy 2013;59:559–69.
[43] Sepman A, Abtahizadeh E, Mokhov A, van Oijen J, Levinsky H, de Goey P. Experimental and numerical studies of the effects of hydrogen addition on the structure of a laminar methane–nitrogen jet in hot coflow under MILD conditions. Int J Hydrogen Energy 2013;38(31):13802–11.
[44] Afarin Y, Tabejamaat S. Effect of hydrogen on H_2/CH_4 flame structure of MILD combustion using the LES method. Int J Hydrogen Energy 2013;38(8):3447–58.
[45] Li P, Dally BB, Mi J, Wang F. MILD oxy-combustion of gaseous fuels in a laboratory-scale furnace. Combust Flame 2013;160(5):933–46.
[46] Li P, Wang F, Mi J, Dally BB, Mei Z. MILD combustion under different premixing patterns and characteristics of the reaction regime. Energy Fuels 2014;28(3):2211–26.
[47] Kumar S, Paul PJ, Mukunda HS. Studies on a new high-intensity low-emission burner. Proc Combust Inst 2002;29(1):1131–7.
[48] Li P, Wang F, Tu Y, Mei Z, Zhang J, Zheng Y, et al. Moderate or intense low-oxygen dilution oxy-combustion characteristics of light oil and pulverized coal in a pilot-scale furnace. Energy Fuels 2014;28(2):1524–35.
[49] Mi J, Li P, Dally BB, Craig RA. Importance of initial momentum rate and air–fuel premixing on MILD combustion in a recuperative furnace. Energy Fuels 2009;23(11):5349–56.
[50] Li P, Mi J. Influence of inlet dilution of reactants on premixed combustion in a recuperative furnace. Flow Turbul Combust 2011;87(4):617–38.
[51] Li P, Mi J, Dally BB, Craig RA, Wang F. Premixed moderate or intense low-oxygen dilution (MILD) combustion from a single jet burner in a laboratory-scale furnace. Energy Fuels 2011;25(7):2782–93.
[52] Mi J, Wang F, Li P, Dally BB. Modified vitiation in a moderate or intense low-oxygen dilution (MILD) combustion furnace. Energy Fuels 2012;26(1):265–77.
[53] ANSYS Fluent 14.0 Documentation. Canonsburg, PA: ANSYS Inc.; 2011.
[54] Gran IR, Magnussen BF. A numerical study of a bluff-body stabilized diffusion flame. Part 2. Influence of combustion modeling and finite-rate chemistry. Combust Sci Technol 1996;119(1–6):191–217.
[55] Smith GP, Golden DM, Frenklach M, Moriarty NW, Eiteneer B, Goldenberg M, et al. GRI-Mech mechanism. http://www.me.berkeley.edu/gri-mech/.
[56] De A, Oldenhof E, Sathiah P, Roekaerts D. Numerical simulation of Delft-jet-in-hot-coflow (DJHC) flames using the eddy dissipation concept model for turbulence–chemistry interaction. Flow Turbul Combust 2011;87(4):537–67.
[57] Aminian J, Galletti C, Shahhosseini S, Tognotti L. Numerical investigation of a MILD combustion burner: analysis of mixing field, chemical kinetics and turbulence-chemistry interaction. Flow Turbul Combust 2012;88(4):597–623.
[58] Christo FC, Dally BB. Modeling turbulent reacting jets issuing into a hot and diluted coflow. Combust Flame 2005;142(1–2):117–29.
[59] De Soete GG. Overall reaction rates of NO and N_2 formation from fuel nitrogen. Proc Combust Inst 1975;15(1):1093–102.
[60] Klippenstein SJ, Harding LB, Glarborg P, Miller JA. The role of NNH in NO formation and control. Combust Flame 2011;158(4):774–89.
[61] De Joannon M, Saponaro A, Cavaliere A. Zero-dimensional analysis of diluted oxidation of methane in rich conditions. Proc Combust Inst 2000;28(2):1639–46.
[62] Minamoto Y, Swaminathan N. Modelling paradigms for MILD combustion. Int J Adv Eng Sci Appl Math 2014:1–11.
[63] Kee RJ, Rupley FM, Miller JA, Coltrin ME, Grcar JF, Meeks E, et al. CHEMKIN release 4.1. San Diego, CA: Reaction Design; 2006.
[64] Mendiara T, Glarborg P. Ammonia chemistry in oxy-fuel combustion of methane. Combust Flame 2009;156(10):1937–49.
[65] Mendiara T, Glarborg P. Reburn chemistry in oxy-fuel combustion of methane. Energy Fuels 2009;23(7):3565–72.
[66] Lee KW, Choi DH. Prediction of NO in turbulent diffusion flames using Eulerian particle flamelet model. Combust Theor Model 2008;12(5):905–27.
[67] Barlow RS, Karpetis AN, Frank JH, Chen JY. Scalar profiles and NO formation in laminar opposed-flow partially premixed methane/air flames. Combust Flame 2001;127(3):2102–18.
[68] Kim SH, Huh KY, Dally B. Conditional moment closure modeling of turbulent nonpremixed combustion in diluted hot coflow. Proc Combust Inst 2005;30(1):751–7.
[69] Kim SH, Huh KY. Use of the conditional moment closure model to predict NO formation in a turbulent CH_4/H_2 flame over a bluff-body. Combust Flame 2002;130(1–2):94–111.
[70] Law CK. Combustion physics. UK: Cambridge University Press; 2006.

[71] Normann F, Andersson K, Leckner B, Johnsson F. Emission control of nitrogen oxides in the oxy-fuel process. Prog Energy Combust Sci 2009;35(5):385–97.
[72] Guo H, Smallwood GJ, Liu F, Ju Y, Gülder ÖL. The effect of hydrogen addition on flammability limit and NO_x emission in ultra-lean counterflow CH_4/air premixed flames. Proc Combust Inst 2005;30(1):303–11.
[73] Turns SR. An introduction to combustion: concepts and applications. New York: McGraw-Hill; 2000.
[74] Dagaut P, Lecomte F. Experiments and kinetic modeling study of NO-reburning by gases from biomass pyrolysis in a JSR. Energy Fuels 2003;17(3):608–13.
[75] Mei Z, Wang F, Li P, Mi J. Diffusion flame of a CH_4/H_2 jet in a hot coflow: effects of coflow oxygen and temperature. Chin J Chem Eng 2013;21(7):787–99.
[76] Wang F, Mi J, Li P. Combustion regimes of a jet diffusion flame in hot co-flow. Energy Fuels 2013;27(6):3488–98.